Journal of Materials Chemistry C

ROYAL SOCIETY OF CHEMISTRY

PAPER

View Article Online
View Journal | View Issue

Check for updates

Cite this: J. Mater. Chem. C, 2025, 13, 15390

Anomalous resistivity and superconductivity in the polymorphs of $(TiZrHf)_{95}Sc_5$

Denver Strong, * Danrui Ni, Xianghan Xu and R. J. Cava*

Received 17th February 2025,
Accepted 4th June 2025

DOI: 10.1039/d5tc00672d

rsc.li/materials-c

Three polymorphs of $(TiZrHf)_{95}Sc_5$, one of which is glassy, are identified. The materials are the result of splat cooling arc melted samples. The temperature-dependent resistivities of the body centered cubic and amorphous materials are anomalous. Low temperature resistivity and heat capacity measurements indicate that superconducting transitions are present when the material has either a body centered cubic ($T_C \sim 1.5$ K) or hexagonal close packed ($T_C \sim 0.8$ K) crystal structure and the superconductivity of the amorphous phase below 0.65 K cannot be ruled out. We include evidence of a robust critical field in the body centered cubic material.

Introduction

High entropy and multicomponent alloys have become increasingly popular over the last decade, primarily due to the fact their stability can be attributed to their large mixing entropy, which can overcome an unfavorable mixing enthalpy.[1] If the mixing entropy does not overcome the enthalpy, then precipitates or mixtures of intermetallic phases can form instead, compromising the possibility of a single solid solution. This high entropy concept has also been used to stabilize intermetallics made from widely different elements, where each site can host a solid solution with little to no atomic mixing between them.[2–4] Furthermore, it has been used as an extension of chemical doping, where the crystal structure is entropically stabilized due to the number of "dopants" but the Fermi energy can be tuned.[1,5,6] The "tunability" associated with multicomponent alloys has opened a vast avenue for studying new electronic and quantum states in materials.

One important advantage of high entropy alloys (HEAs) is the fact that the competition between entropy and enthalpy can stabilize *new* phases. One path where exploration has been limited has been the study of polymorphs of the same composition with different physical and electronic structures. Due to the number of binary interactions at play, adjusting the temperature or pressure of a material with a single composition gives the field of materials physics access to study the consequences of polymorphism.[7] One review paper emphasized the importance of elements, structure, and synthesis to compare materials one-to-one, and entropy stabilized materials offer a promising route to such control.[8]

Department of Chemistry Princeton University, Princeton, NJ, USA.
E-mail: dpstrong@princeton.edu, rcava@princeton.edu

For superconducting high entropy alloys in general, a few reports stand out as being relevant to the current work. First, are two series (Nb-Mo-Re-Ru-Rh and Mo-W-Re-Ru-Pd) where the relative concentrations can be changed to stabilize various crystal structures (α-Mn → Hexagonal Close Packed (HCP) and Body Centered Cubic (BCC) → σ → HCP, respectively).[9,10] All were reported to show fully gapped superconducting states and a clear linear trend in the superconducting transition temperature (T_C) even across structure types, indicating a subtle difference in their density of states at the Fermi energy. Closer to the current work is the explicit polymorphism in superconducting V-Nb-Mo-Al-Ga, comparing the as-cast body centered cubic solid solution and the annealed, ordered A15-type material - the latter of which superconducts below a Tc of 10 K while the as-cast body centered cubic version shows no sign of superconductivity above 2 K.[11] Here we report the existence of multiple polymorphs, one of which is amorphous, of a single medium entropy alloy, and signs of very low temperature superconductivity in the crystalline materials.

Methods

Because the entropic contributions to the free energy are maximized at high temperature, high temperature synthesis and fast cooling were employed. The nominal formula for the hexagonal close packed (HCP) sample was $(TiZrHf)_{95}Sc_5$ while the beginning composition for body centered cubic (BCC) sample was $(TiZrHf)_{90}Sc_{10}$. The amount of material summed to 200 mg and 300 mg for the HCP and BCC samples respectively. Stoichiometric amounts of Ti, Zr, and Hf powders were compressed using a steel dye and Sc pieces were melted alongside the resulting pellet.

The samples were placed in the arc melter alongside a Zr getter, which was heated to collect any residual oxygen in the

chamber. The samples were originally melted with a low current to sinter the powders into a more robust pellet. The power was then increased to melt each sample into a button: I ≈ 50 A and V ≈ 480 V was usually sufficient. Once in the molten state, it was held there for 5–8 seconds. Each sample was melted 3–5 times and flipped in between to ensure homogeneity. Mass loss in the HCP sample was negligible and mass loss in the BCC sample neared 2.5%. Some of the Sc boiled away in the preparation of the BCC material due to the fact that temperatures exceeding 3100 °C were obtained.

Afterward, the resulting buttons were placed in a water-cooled copper well. Residual oxygen was once again collected with a Zr getter. The sample was heated for 5–8 seconds after reaching the molten state. Immediately after that time, the electrode was withdrawn from the well and a spring-loaded Cu plate was released to rapidly cool the sample. (*i.e.* splat cooling to maintain the high entropy state) The result was thin solidified sheets with variable morphology.

Since the samples were typically thin, powder X-ray diffraction (pXRD) measurements can be collected easily. Diffractograms were collected in the Bragg Brentano geometry on a Bruker D8 Advance ECO diffractometer using Cu Kα X-rays. Le Bail refinements were performed using GSAS-II to determine lattice parameters. A Quanta 200 FEG Environmental Scanning Electron Microscope (SEM) equipped with Energy-dispersive X-Ray spectroscopy (EDS) was also used to confirm the stoichiometry of select samples.

Physical property measurements were performed in a Quantum Design Physical Property Measurement System (PPMS) equipped with a ^{3}He apparatus. Resistivity measurements were performed on a 4-probe resistivity puck between 0.3 K and 300 K. Heat capacity measurements were done between 0.65 K and 200 K.

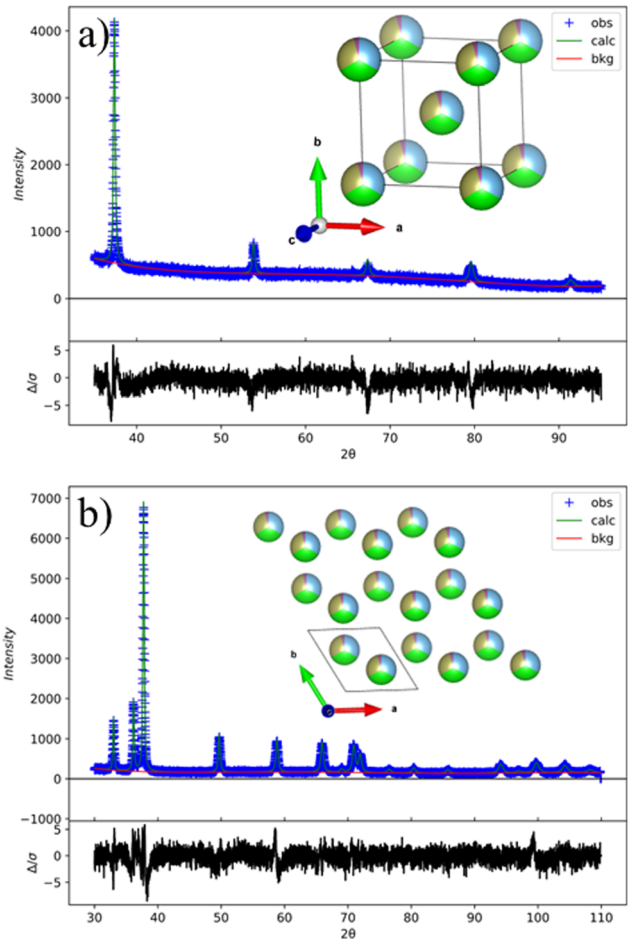

Fig. 1 Bulk polycrystalline X-ray diffraction patterns for the (a) BCC and (b) HCP phases. (Cu Kα radiation) Their relative structures are presented as well showing 31.7% Ti, 31.7% Zr, 31.7% Hf, and 5% Sc.

Structure & morphology

Fig. 1 reports two crystalline structures arising from splat cooling. The first of which, hexagonal close packed (HCP), the structure-in-structure-out method predicts;[1] however, the refined lattice parameters, a = 3.1468(2) A and c = 4.9864(2) A, are slightly larger than the weighted average of the individual elements' lattice parameters. The other crystalline material is body centered cubic (BCC) with lattice parameter, a = 3.4067(2) A.

High temperature BCC allotropes of the groups III and IV elements have been reported and a calculated phase diagram suggests the ternary TiZrHf BCC phase exists as well with a minimum suggested heating temperature of 1200 °C.[12–16] The type of splat cooling used here is meant to stabilize high temperature and metastable phases by creating a thin sample, quenched between two plates that absorb heat quickly. General arc melting can exceed 3000 °C given by the fact it can reliably melt W and Re. Although the nominal composition of the BCC sample was $(TiZrHf)_{90}Sc_{10}$, the EDS measurements, shown in Fig. 2a, confirmed an actual composition of $(TiZrHf)_{95}Sc_5$ which is likely due to reaching temperatures exceeding 3100 °C for this sample.

The surface morphologies of the bulk pieces in Fig. 2 immediately indicate the quality of the splat, as the BCC sample is much smoother. The experimentally determined composition of (a) is $Ti_{30.9}Zr_{32.2}Hf_{32.7}Sc_{4.3}$ while the experimentally determined composition of (b) is $Ti_{30.9}Zr_{30.3}Hf_{34.5}Sc_{4.3}$. (The missing data for the HCP sample is due to the surface morphology where higher parts of the sample block the path between the sample and the detector.) Local spectra on the latter consistently returned scandium concentrations between 3.4% and 4.5% suggesting that the material is compositionally homogenous.

In order to perform the physical property measurements, small pieces (<2 mg) were broken off the edges of the bulk splats. Since these are high temperature phases, pXRD was run on every piece and, during this process, an additional amorphous phase was found in both samples, which contributed to the strong background shown in Fig. 3. Unfortunately, the splat cooling apparatus used here is not capable of isolating the three phases. With this in mind, EDS measurements were performed on any piece where physical property measurements were done to confirm its composition. While transmission electron microscopy (TEM) would be ideal for identifying each structure, it's difficult for the electron beam to pass through the bulk material. In previous work, we've used TEM on powder

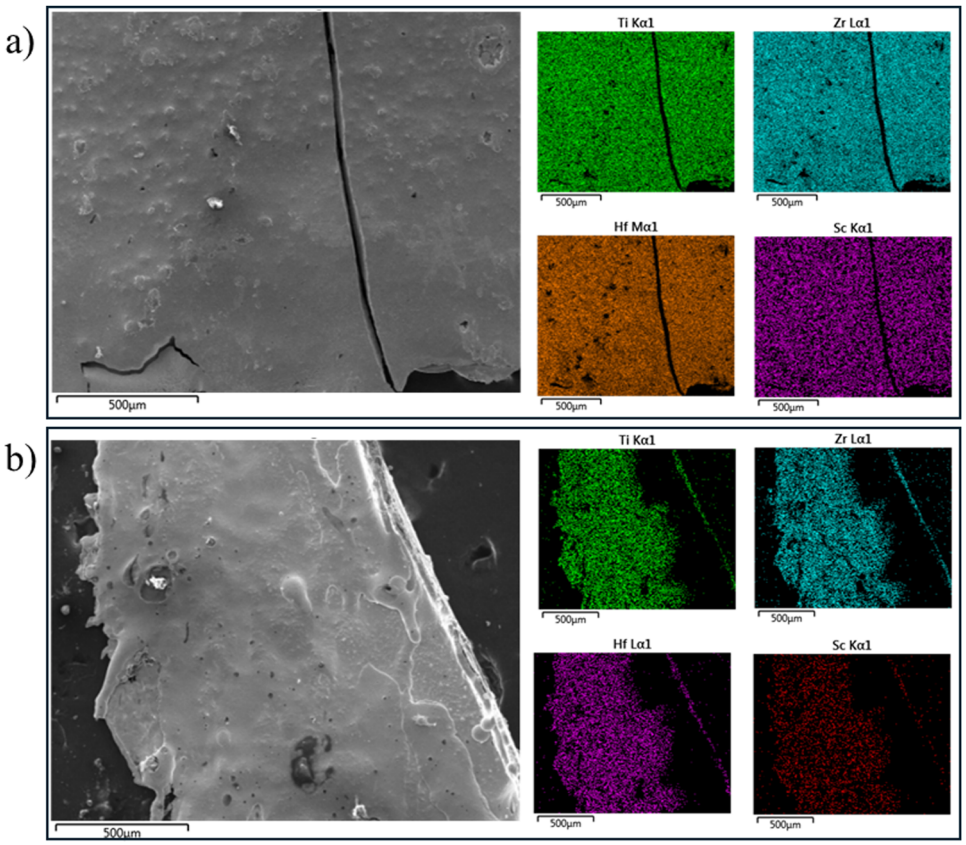

Fig. 2 Energy dispersive spectroscopy measurements for (a) BCC and (b) HCP pieces. Data is limited on the surface of (b) due to the surface morphology blocking the electron beam. The elemental compositions of each sample generally agree with Ti ~ 31%, Zr ~ 32%, Hf ~ 33%, and Sc ~ 4%. The scale bar is 500 μm.

samples filed from the bulk and many of those particles were still too large due to the fact that HEAs are much harder than traditional metals.[17]

Discovering the amorphous component was a surprise; however, Zr- and Hf-based alloys tend to be reliable glass formers in conjunction with a later transition metal such as Ni or Cu.[18–20] Ti-Zr-Hf has been included in other high entropy and bulk metallic glasses, but to the best of our knowledge, they have yet to be reported exclusively within the early transition metals.[19,21–28] Many of these amorphous alloys are synthesized using melt spinning which has a lower cooling rate than the method used here.[29,30]

Since the samples reported here physically appear to be splatted in some form or another, it's obvious the Cu splat tip is impacting the material while it's still in the molten state. We suggest the following explanation for the formation of the polymorphs. If the impact occurs while the sample is at different temperatures, the viscosities of each will differ. An impact at a higher sample temperature where the molten liquid can flow more freely, will in turn increase the surface contact area, cooling the sample faster, stabilizing the high temperature state. We presume the amorphous component forms during the initial contact at the interface of the copper and sample explaining why there seems to be weaker crystalline peaks in the small pieces measured; however, a dedicated and systematic study of this mechanism would be beneficial.

Our work emphasizes the importance of two-tier cooling during this process. While in the molten state, the cooling should be "slow" to initialize a higher effective temperature after impact. One way to do this is by varying the mass of the melt. Larger samples cool slower, enhancing the quality of the splat after impact. This is the opposite of traditional arc melting considering smaller samples are often used to get the fastest cooling rate.

Resistivity

Superconductivity was observed in two of the three polymorphs discussed here, which is summarized in Fig. 4. The resistivity for the HCP variant is included in Fig. 4a and decreases with decreasing temperature before it flattens near 50 K. The residual resistivity ratio, $\rho_{300\ K}/\rho_{2\ K}$ = 1.59, is on par with other concentrated alloys.[31–33] It's interesting to note the values reported here are very similar to ScTiZrHf which was arc melted then annealed for 140 hours at 700 °C.[31] This may suggest the microstructures, which can affect resistivity due to grain boundaries, are not very different between the two synthesis methods. The superconducting transition for our alloy can be seen near 1.0 K.

Fig. 4b shows data for a piece of the BCC sample with a superconducting transition near 1.5 K. Above the transition,

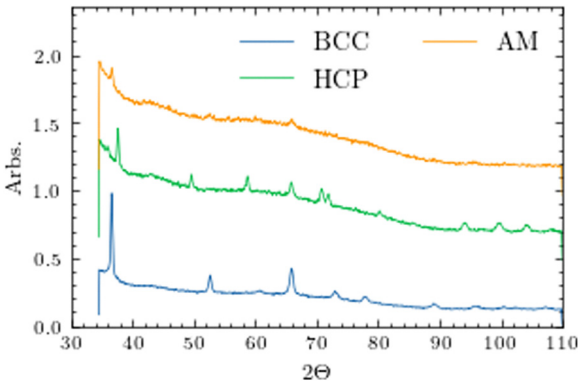

Fig. 3 X-Ray diffraction patterns for the primarily BCC (blue), HCP (green), and amorphous (AM – yellow) phases. Data was smoothed with a 10-point simple moving average to improve clarity before normalization. (Cu Kα radiation) The large dome-like background present in each scan is presumed to be an underlying amorphous phase limiting our ability to do quantitative analysis.

the shape of the resistivity curve is anomalous. The primary feature is decreasing resistivity with increasing temperature, indicated with the dashed line. This has been reported in other glassy materials with resistivities between 150–300 μΩ cm and arises because the mean free path of the electrons is on the order of the interatomic distances.[34–36] This phenomenon, often called the Mooij rule, has been explained using weak localization effects.[37,38] At this level, the intercarrier distance is on the order of the interatomic spacing. Here, the electrons are essentially 'trapped' near one atom and the material begins to act like an insulator. This is often seen in metallic glasses with a low carrier concentration and is being realized more in disordered glassy alloys.[39–41]

Of particular importance is why this anomalous curve is observed instead of the standard metallic behavior of BCC alloys. Since the BCC resistivity in Fig. 4d does go to zero, there is a complete superconducting path between the voltage leads – within experimental error. There's no evidence here or in the literature that this transition is associated with the amorphous phase, otherwise, a small superconducting signature would be present in the HCP sample as well. Often it is seen that the BCC structure has a lower resistivity than the HCP counterpart. This can be seen when comparing the group IV and V transition metals as well as a decrease in resistivity once Ti, Zr, and Hf undergo their structural change to BCC at high temperatures.[42–44] Unfortunately, resistivity data for the BCC allotropes at 300 K could not be found for comparison.

While there are very few examples of crystalline metals displaying this type of behavior, it's well recorded that atomic disorder can contribute to a negative temperature dependence in resistivity.[45,46] This may be one realization where high entropy alloys with very few carriers induce an anomalous effect, but measurements on BCC Ti, Zr, or Hf below 300 K are required to confirm this behavior is driven by disorder.

It's important to note the magnitude of the resistivity as well. At 585 μΩ cm, it is surprising there is not an underlying metallic behavior. Many HEAs have resistivities of 100–200 μΩ cm[47–51] but there are reports of σ-phase HEAs reaching 400 μΩ cm and α-Mn types nearing 600 μΩ cm.[48,52] While microstructure and grain boundaries can increase the resistance, another cause that cannot be ruled out is that the conduction path length is incorrect. This is particularly important in multiphase samples where the current may have to take many detours before reaching the other voltage lead. However, this is not expected to reverse the trend which is seen above 150 K.

Focusing on the superconducting transitions, in agreement with previous literature, the HCP phase has the lower transition temperature, (T_C), plotted in Fig. 4c. At zero field, the 50% criterion indicates T_C = 0.98 K whereas the BCC phase has a transition centered at 1.5 K (Fig. 4d.) Following this, an analysis to determine the critical field was done on each material.

We plot the superconducting temperatures at each applied field to estimate the upper critical field at 0 K, $H_{c2}(0)$. We include additional points representing the absolute maximum field due to the Zeeman energy,[53] $H_{max} = 2.6T_C$, another for the Pauli paramagnetic limit,[54] $H_P = 1.84T_C$ and finally the Werthamer–Helfand–Hohenberg (WHH) theory,[55–59]

$$\mu_0 H_{c2}(0) = -0.693\mu_0 \left(\frac{dH}{dT}\right)_{T=T_C} T_C, \quad (1)$$

which introduces the self-destructive paramagnetic and spin–orbit effects. The latter uses the slope in the H–T phase diagram evaluated at the zero-field transition temperature. For the three limits, the HCP sample returns 2.55 T, 1.80 T, and 0.62 T, respectively; while applying the models to the BCC phase returns 3.90 T, 2.76 T, and 1.30 T; all of which are plotted within Fig. 4e and f.

Two additional models are presented as well. Model 1 (red),[2,60,61]

$$H_{c2}(T) = H_{c2}(0)\left(1 - t^{\frac{3}{2}}\right)^{\frac{3}{2}}, \quad (2)$$

and model 2 (green),[51,62,63]

$$H_{c2}(T) = H_{c2}(0)\frac{1-t^2}{1+t^2}, \quad (3)$$

where $t = T/T_C$. Both have been used for superconducting HEAs before. For the HCP sample, $H_{c2}(0)$ = 0.83 T and 0.70 T, respectively. While both are near the WHH approximation from eqn (1), with only three points, it's not possible to tell which model is more appropriate. For the BCC sample, $H_{c2}(0)$ = 3.42 T and 2.96 T, respectively, where model 1 seems to be a better fit to the data with R^2 = 0.997. Importantly, for the BCC phase, both models seem to exceed the Pauli limit, H_P = 2.76 T. It was recently reported that another BCC HEA, equimolar ScVTiHfNb,[51] also demonstrates an enhanced upper critical field. This effect has been observed in many of our own related compounds as well which are to be published elsewhere.

The Zeeman splitting induced by a magnetic field is the primary mechanism to destroy superconductivity.[53] However, an applied field also raises the energy of spin-down electrons. This means any carriers that were anti-aligned with the applied field will have some

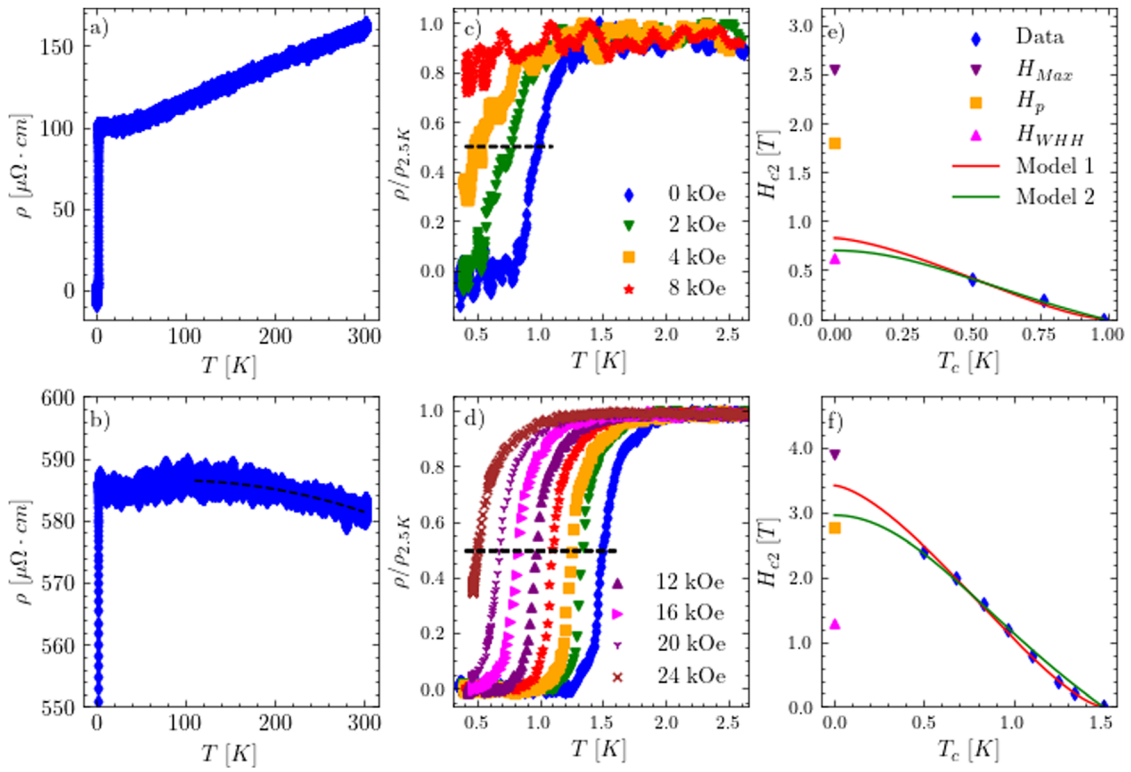

Fig. 4 Resistivity data for the HCP material (top) and the BCC material (bottom). (a) and (b) show resistivity measurements between 300 K and 0.3 K. (c) and (d) show the transition temperature in resistivity becoming suppressed with applied field. The legend is split between the two panels for clarity. (e) and (f) show the superconducting phase diagrams. A description of the models is outlined in the text. The legend is the same for both panels. There are not enough data points to appropriately characterize the HCP phase.

inclination to flip. This induces Pauli paramagnetism which is self-destructive to the superconducting state (*i.e.* The Pauli limit).[54] We propose two hypotheses for the robust critical field, both of which require a more detailed theoretical analysis to confirm.

Hypothesis 1

Pauli paramagnetism is directly related to the density of states at the Fermi energy, $\chi_P = \mu_B{}^2 g(E_F)$, where μ_B is the Bohr magneton. It's reasonable to suggest there is a minimal number of carriers in these systems simply because the valence electron count (VEC) < 4. Without a substantial number of carriers, these materials minimize compounding effects from the self-induced magnetic field, pushing the boundaries of the Pauli limit.

Hypothesis 2

It's been reported that transition metals want to maximize the spin of the system (Hund's rules).[64] With such few total carriers, most of these electrons are already pointing the same direction and, in return, it takes very little energy to reorient the few orphan electrons. If nothing is reoriented, there are no self-destructive tendencies. As a follow up to this concept, the initial upward curvature in Fig. 4f is a fundamental feature of charged bosons.[60] If it's taken that a cooper pair is a boson, but the correlated electrons are both spin up, the cooper pair in these materials are charged.

It is important that we address the potential impact of the mixed phases on the superconducting properties. It's previously been reported that eutectic phases can influence the mechanical properties of high entropy alloys as well as increase their superconducting transition temperatures.[65,66] This was related to the proximity effect but does not seem to be relevant to the superconducting phases reported here primarily because amorphous phases with low VECs have lower transition temperatures than their crystalline counterparts.[67] However, the proximity effect may be relevant for the transition temperature of the amorphous phase if it does superconduct; which specific heat measurements would be required to confirm. Beyond this, eutectic phases have been shown to enhance the critical current compared to the bulk. This is because the critical current is intricately related to the microstructure as well as the nature of the eutectic phases.[68] However, the literature suggests this enhanced critical current is not followed by an enhanced critical field because the underlying electronic structure is not significantly changed,[69] indicating the enhanced critical fields are not trivial and more detailed work needs to be done on low VEC HEAs.

Heat capacity

Since previous measurements confirm the potential for multi-phase pieces, specific heat measurements (Fig. 5) are used to identify an anomaly near the transition temperature, but a quantitative analysis of the superconducting jump would not be insightful without a pure phase.

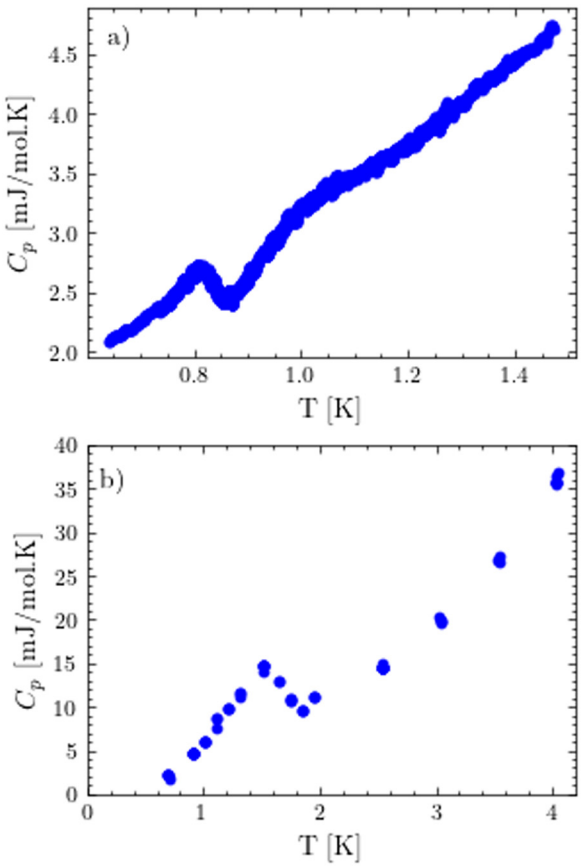

Fig. 5 The superconducting anomaly in the (a) HCP and (b) BCC materials. Since the transition temperature of the HCP system is near the reliable limit of the ^{3}He apparatus, Quantum Design's dual slope analysis routine was used, which gives more data points.

Data for the HCP sample is shown in Fig. 5a. A jump associated with the transition temperature occurs near 0.8 K, reasonably just below the transition in the resistivity. Since the transition temperature is near the reliable limit of the He^3 apparatus, Quantum Design's dual slope analysis routine was used which gives more data points.

The results for the BCC material are reported in Fig. 5b. The well-defined peak of the anomaly near 1.5 K is consistent with resistivity measurements. Fitting the high temperature region to the Einstein model,

$$\frac{C_p}{T} = \gamma + \beta T^2, \quad (4)$$

returns an electronic contribution, γ = 3.1521 mJ mol^{-1} K^{-2}, and a phonon contribution with β = 0.12092 mJ mol^{-1} K^{-4}. Translating the latter value into a Debye temperature with

$$\theta_D = \sqrt[3]{\frac{12\pi^4 k_B N}{5\beta}} = 252 \text{ K} \quad (5)$$

is on par with values found for both structures using the Debye model between 1 K and 60 K (not shown). Here, k_B is the Boltzmann constant, and N is Avogadro's number. The Debye temperature should be similar between the two crystalline materials since it's strongly related to the speed of sound in a material and is heavily dependent on the weight of the atoms. However, amorphous materials do not follow a T^3 dependence at low temperatures, so rigorous calculations cannot be done.[70]

Conclusion

We've synthesized mixed phase HCP + amorphous and BCC + amorphous versions of the $(TiZrHf)_{95}Sc_5$ medium entropy alloy. We also showed the possibility of targeting polymorphs by splat cooling arc melted samples and taking advantage of a two-tiered cooling process. Superconducting signals were shown for the crystalline phases with the HCP phase at 0.98 K and the BCC phase at 1.5 K. The latter has a critical field that exceeds the Pauli limit. Superconductivity of the amorphous phase below 0.65 K cannot be ruled out. These results encourage further exploration of low VEC HEAs and the splat cooled arc melting technique may significantly expand the number of entropy-stabilized alloys that appear to display superconductivity.

Author contributions

Conceptualization, synthesis, and limited structural and physical property characterizations were performed by Denver Strong. SEM measurements were done by Danrui Ni. Low temperature PPMS experiments were performed by Xianghan Xu. R. J. Cava funded and directed the work.

Ethical approval

Not applicable

Data availability

Please reach out to the corresponding author for raw data. It's also available at **https://github.com/dpstrong/Polymorph-Data_Ti-Zr-Hf-Sc**.

Conflicts of interest

There are no conflicts of interest.

Acknowledgements

This research was funded by the Gordon and Betty Moore Foundation, grant number GBMF-9066, and by the Division of Basic Energy Sciences of the US Department of Energy, grant number DE-FG02-98ER-45706.

References

1 D. B. Miracle and O. N. Senkov, A critical review of high entropy alloys and related concepts, *Acta Mater.*, 2017, **122**, 448–511.

2 K. Stolze, J. Tao, F. O. Von Rohr, T. Kong and R. J. Cava, Sc–Zr–Nb–Rh–Pd and Sc–Zr–Nb–Ta–Rh–Pd High-Entropy Alloy Superconductors on a CsCl-Type Lattice, *Chem. Mater.*, 2018, **30**, 906–914.
3 B. Liu, *et al.*, Superconductivity in Cubic A15-type V–Nb–Mo–Ir–Pt High-Entropy Alloys, *Front. Phys.*, 2021, **9**, 651808.
4 A. Yamashita, *et al.*, An efficient way of increasing the total entropy of mixing in high-entropy-alloy compounds: a case of NaCl-type (Ag,In,Pb,Bi)$Te_{1-x}Se_x$ (x = 0.0, 0.25, 0.5) superconductors, *Dalton Trans.*, 2020, **49**, 9118–9122.
5 D. Strong and R. J. Cava, Superconductivity in the face-centered cubic W-M-Rh-Ir-Pt M = {Mo, Nb, Ta, Re} high-entropy alloy, *J. Mater. Sci.*, 2024, **59**, 10347–10356.
6 L. Zeng, *et al.*, Superconductivity and non-trivial band topology in high-entropy carbonitride $Ti_{0.2}Nb_{0.2}Ta_{0.2}Mo_{0.2}W_{0.2}C1-xNx$, *Innovation Mater.*, 2023, **1**, 100042.
7 F. Zhang, *et al.*, Polymorphism in a high-entropy alloy, *Nat. Commun.*, 2017, **8**, 15687.
8 T. Berry, N. Ng and T. M. McQueen, Tools and Tricks for Single Crystal Growth, *Chem. Mater.*, 2024, **36**, 4929–4944.
9 B. Liu, *et al.*, Structural evolution and superconductivity tuned by valence electron concentration in the Nb–Mo–Re–Ru–Rh high-entropy alloys, *J. Mater. Sci. Technol.*, 2021, **85**, 11–17.
10 X. Xu, *et al.*, Structural sequence and superconductivity in high-entropy Mo–W–Re–Ru–Pd alloys, *Scr. Mater.*, 2024, **243**, 115986.
11 J. Wu, *et al.*, Polymorphism and superconductivity in the V-Nb-Mo-Al-Ga high-entropy alloys, *Sci. China Mater.*, 2020, **63**, 823–831.
12 W. Petry, *et al.*, Phonon dispersion of the bcc phase of group-IV metals. I. bcc titanium, *Phys. Rev. B:Condens. Matter Mater. Phys.*, 1991, **43**, 10933–10947.
13 A. Heiming, *et al.*, Phonon dispersion of the bcc phase of group-IV metals. II. bcc zirconium, a model case of dynamical precursors of martensitic transitions, *Phys. Rev. B:Condens. Matter Mater. Phys.*, 1991, **43**, 10948–10962.
14 J. Trampenau, *et al.*, Phonon dispersion of the bcc phase of group-IV metals. III. bcc hafnium, *Phys. Rev. B: Condens. Matter Mater. Phys.*, 1991, **43**, 10963–10969.
15 C. Stassis, J. Zarestky and N. Wakabayashi, Lattice Dynamics of bcc Zirconium, *Phys. Rev. Lett.*, 1978, **41**, 1726–1729.
16 L. Lin, L. Delaey, O. Van Der Biest and P. Wollants, Calculation of isothermal sections of three ternary Ti–Zr–X systems, *Scr. Mater.*, 1996, **34**, 1411–1416.
17 A. J. Browne, D. P. Strong and R. J. Cava, Phase stability and possible superconductivity of new 4d and 5d transition metal high-entropy alloys, *J. Solid State Chem.*, 2023, **321**, 123881.
18 F. E. Luborsky, *Amorphous metallic alloys*, Elsevier Science, Kent, 2014.
19 R. Ristić, *et al.*, Properties and atomic structure of amorphous early transition metals, *J. Alloys Compd.*, 2010, **504**, S194–S197.
20 I. Bakonyi, Electronic properties and atomic structure of (Ti, Zr, Hf)(Ni, Cu) metallic glasses, *J. Non-Cryst. Solids*, 1995, **180**, 131–150.
21 A. Pasko, *et al.*, Crystallization of the amorphous phase and martensitic transformations in multicomponent (Ti,Hf,Zr)-(Ni,Cu)-based alloys, *J. Non-Cryst. Solids*, 2007, **353**, 3062–3068.
22 M. Hasiak, *et al.*, Some Magnetic Properties of Bulk Amorphous Fe–Co–Zr–Hf–Ti–W–B–(Y) Alloys, *IEEE Trans. Magn.*, 2008, **44**, 3879–3882.
23 L. Wang, C. Li and A. Inoue, Formation of Ti-Zr(Hf)-Ni-Cu Amorphous Alloys and Quasicrystal Precipitation upon Annealing, *Mater. Trans.*, 2001, **42**, 528–531.
24 Y. J. Huang, J. Shen, J. F. Sun and X. B. Yu, A new Ti–Zr–Hf–Cu–Ni–Si–Sn bulk amorphous alloy with high glass-forming ability, *J. Alloys Compd.*, 2007, **427**, 171–175.
25 R. Ristić, *et al.*, Transition from high-entropy to conventional $(TiZrNbCu)_{1-x}Co_x$ metallic glasses, *J. Appl. Phys.*, 2021, **130**, 195102.
26 A. Inoue, K. Kobayashi, M. Nose and T. Masumoto, Mechanical properties of (Fe, Co, Ni)-M-B (M = Ti, Zr, Hf, V, Nb, Ta AND Mo) amorphous alloys with low boron concentration, *J. Phys., Colloq.*, 1980, **41**, C8-831–C8-834.
27 H. Son, G. Yoo, Q. Mustaghfiroh, D.-H. Kim and H. Choi-Yim, Effect of Substituting Hf for Zr on Fe-Co-M-Nb-B (M = Zr, Hf) Amorphous Alloys with High Saturation Magnetization, *Metals*, 2021, **12**, 12.
28 R. Ristić, K. Zadro, D. Pajić, I. A. Figueroa and E. Babić, On the origin of bulk glass forming ability in Cu-Hf, Zr alloys, *EPL Europhys. Lett*, 2016, **114**, 17006.
29 K. Biljaković, *et al.*, Electronic structure and properties of $(TiZrNbCu)_{1-x}Ni_x$ high entropy amorphous alloys, *J. Alloys Compd.*, 2017, **695**, 2661–2668.
30 I. A. Figueroa, *et al.*, Properties of $(TiZrNbCu)_{1-x}Ni_x$ metallic glasses, *J. Alloys Compd.*, 2018, **745**, 455–459.
31 S. Uporov, S. Kh Estemirova, V. A. Bykov, D. A. Zamyatin and R. E. Ryltsev, A single-phase ScTiZrHf high-entropy alloy with thermally stable hexagonal close-packed structure, *Intermetallics*, 2020, **122**, 106802.
32 S. Marik, *et al.*, Superconductivity in a new hexagonal high-entropy alloy, *Phys. Rev. Mater.*, 2019, **3**, 060602.
33 B. Liu, *et al.*, Superconductivity in hexagonal Nb-Mo-Ru-Rh-Pd high-entropy alloys, *Scr. Mater.*, 2020, **182**, 109–113.
34 D. Korn, H. Pfeifle and G. Zibold, Electrical resistivity of amorphous alloys, *Z. Für Phys*, 1974, **270**, 195–202.
35 K. Frobose and J. Jackle, On the temperature dependence of the electrical resistivity of amorphous metals, *J. Phys. F: Met. Phys.*, 1977, **7**, 2331–2348.
36 S. R. Nagel, Temperature dependence of the resistivity in metallic glasses, *Phys. Rev. B: Solid State*, 1977, **16**, 1694–1698.
37 J. H. Mooij, Electrical conduction in concentrated disordered transition metal alloys, *Phys. Status Solidi A*, 1973, **17**, 521–530.
38 V. F. Gantmakher, Mooij rule and weak localization, *JETP Lett.*, 2011, **94**, 626–628.
39 V. F. Gantmakher and L. I. Man, *Electrons and Disorder in Solids*, Oxford University Press, 2005, DOI: **10.1093/acprof:oso/9780198567561.001.0001**.

40 M. Park, K. Savran and Y. Kim, Weak localization and the Mooij rule in disordered metals, *Phys. Status Solidi B*, 2003, **237**, 500–512.
41 S. Ciuchi, D. Di Sante, V. Dobrosavljević and S. Fratini, The origin of Mooij correlations in disordered metals, *Npj Quantum Mater.*, 2018, **3**, 44.
42 W. C. Michels and S. Wilford, The Physical Properties of Titanium. I. Emissivity and Resistivity of the Commercial Metal, *J. Appl. Phys.*, 1949, **20**, 1223–1226.
43 A. Cezairliyan and F. Righini, Thermodynamic studies of the a? phase transformation in zirconium using a subsecond pulse heating technique, *J. Res. Natl. Bur. Stand. Sect. Phys. Chem*, 1975, **79A**, 81.
44 P. D. Desai, T. K. Chu, H. M. James and C. Y. Ho, Electrical Resistivity of Selected Elements, *J. Phys. Chem. Ref. Data*, 1984, **13**, 1069–1096.
45 T. Harmening, H. Eckert and R. Pöttgen, Defects in half-Heusler type antimonides ScTSb (T = Ni, Pd, Pt), *Solid State Sci.*, 2009, **11**, 900–906.
46 D. Gnida, K. Ciesielski and D. Kaczorowski, Origin of the negative temperature coefficient of resistivity in the half-Heusler antimonides LuNiSb and YPdSb, *Phys. Rev. B*, 2021, **103**, 174206.
47 F. Von Rohr, M. J. Winiarski, J. Tao, T. Klimczuk and R. J. Cava, Effect of electron count and chemical complexity in the Ta–Nb–Hf–Zr–Ti high-entropy alloy superconductor, *Proc. Natl. Acad. Sci. U. S. A.*, 2016, **113**, E7144–E7150.
48 K. Stolze, F. A. Cevallos, T. Kong and R. J. Cava, High-entropy alloy superconductors on an α-Mn lattice, *J. Mater. Chem. C*, 2018, **6**, 10441–10449.
49 M.-H. Tsai, Physical Properties of High Entropy Alloys, *Entropy*, 2013, **15**, 5338–5345.
50 J. Kitagawa, *et al.*, Superconductivity and hardness of the equiatomic high-entropy alloy HfMoNbTiZr, *J. Alloys Compd.*, 2022, **924**, 166473.
51 S. Jangid, *et al.*, Superconductivity with a high upper critical field in an equiatomic high-entropy alloy Sc–V–Ti–Hf–Nb, *Appl. Phys. Lett.*, 2024, **124**, 192602.
52 B. Liu, *et al.*, Formation and Superconductivity of Single-Phase High-Entropy Alloys with a Tetragonal Structure, *ACS Appl. Electron. Mater*, 2020, **2**, 1130–1137.
53 B. S. Chandrasekhar, A note on the Maximum critical field of high-field superconductors, *Appl. Phys. Lett.*, 1962, **1**, 7–8.
54 A. M. Clogston, Upper Limit for the Critical Field in Hard Superconductors, *Phys. Rev. Lett.*, 1962, **9**, 266–267.
55 R. R. Hake, Paramagnetic Superconductivity in Extreme Type-II Superconductors, *Phys. Rev.*, 1967, **158**, 356–376.
56 E. Helfand and N. R. Werthamer, Temperature and Purity Dependence of the Superconducting Critical Field, H_c^{2II}, *Phys. Rev.*, 1966, **147**, 288–294.
57 N. R. Werthamer, E. Helfand and P. C. Hohenberg, Temperature and Purity Dependence of the Superconducting Critical Field, H_{c2}. III. Electron Spin and Spin-Orbit Effects, *Phys. Rev.*, 1966, **147**, 295–302.
58 R. R. Hake, Upper-critical-field limits for bulk type-II superconductors, *Appl. Phys. Lett.*, 1967, **10**, 189–192.
59 G. Cody, *Critical fields of type II superconductors*, RCA Laboratories Princeton, New Jersey, 1968, pp. 405–436.
60 R. Micnas, J. Ranninger and S. Robaszkiewicz, Superconductivity in narrow-band systems with local nonretarded attractive interactions, *Rev. Mod. Phys.*, 1990, **62**, 113–171.
61 A. B. Karki, *et al.*, Physical properties of the noncentrosymmetric superconductor $Nb_{0.18}Re_{0.82}$, *Phys. Rev. B: Condens. Matter Mater. Phys.*, 2011, **83**, 144525.
62 G. Xiao, *et al.*, Chemical composition effect on superconductivity in noncentrosymmetric β -Mn-type high-entropy alloys, *J. Mater. Res. Technol.*, 2024, **28**, 2516–2522.
63 G. Kim, *et al.*, Strongly correlated and strongly coupled s-wave superconductivity of the high entropy alloy Ta1/6Nb2/6Hf1/6Zr1/6Ti1/6 compound, *Acta Mater.*, 2020, **186**, 250–256.
64 S. K. Riddle, T. R. Wilson, M. Rajivmoorthy and M. E. Eberhart, Principles Determining the Structure of Transition Metals, *Molecules*, 2021, **26**, 5396.
65 J. Kitagawa, N. Ishizu and S. Hamamoto, Materials Research on High-Entropy Alloy Superconductors, in *Advances in High-Entropy Alloys – Materials Research, Exotic Properties and Applications*, ed., J. Kitagawa, IntechOpen, 2021, DOI: **10.5772/intechopen.99693**.
66 Y. Lu, *et al.*, A Promising New Class of High-Temperature Alloys: Eutectic High-Entropy Alloys, *Sci. Rep.*, 2014, **4**, 6200.
67 C. A. Shiffman, J. F. Cochran, M. Garber and G. W. Pearsall, Specific Heat Measurements and Proximity Effects in Tin-Lead Eutectic Alloys, *Rev. Mod. Phys.*, 1964, **36**, 127–130.
68 J. E. Evetts, A. M. Campbell and D. Dew-hughes, Flux instabilities in hard superconductors, *Philos. Mag.*, 1964, **10**, 339–343.
69 S. A. Levy, Y. B. Kim and R. W. Kraft, Effect of Structure on the Superconducting Properties of Eutectic Alloys, *J. Appl. Phys.*, 1966, **37**, 3659–3665.
70 R. E. Newnham, *Properties of Materials: Anisotropy, Symmetry, Structure*, Oxford University Press, Oxford, New York, 2005.